Mechanical Property Correlation and Laser Parameter Development for the Selective Laser Sintering of Carbon Fiber Reinforced Polyetheretherketone

Scott E. Snarr, Joseph J. Beaman Jr., Scott Fish
Department of Mechanical Engineering, The University of Texas at Austin, Austin, TX 78751

Chapter 1. Introduction

Recent advancements in Additive Manufacturing (AM) have led to an increased interest in the use of AM for constructing production quality parts. Selective Laser Sintering is one candidate for building parts that meet these high standards, but improvements to the procedure's material capabilities, process control, and predictive modeling are necessary. Selective Laser Sintering (SLS) is a layer-based process where a roller spreads an approximately .1 mm (100 micron) layer of powder over a piston. A laser then traces out a 2-D cross sectional area, depositing enough energy to raise the powder particles above their melting temperature. This allows the particles to fuse together and form bonds with their neighboring particles. The piston then lowers and another layer of powder is spread over top of the previously sintered one. This process is then repeated many times until the desired three-dimensional object is created (Beaman Jr. & Deckard, 1990). A detailed image of the SLS process is shown below in Figure 1.
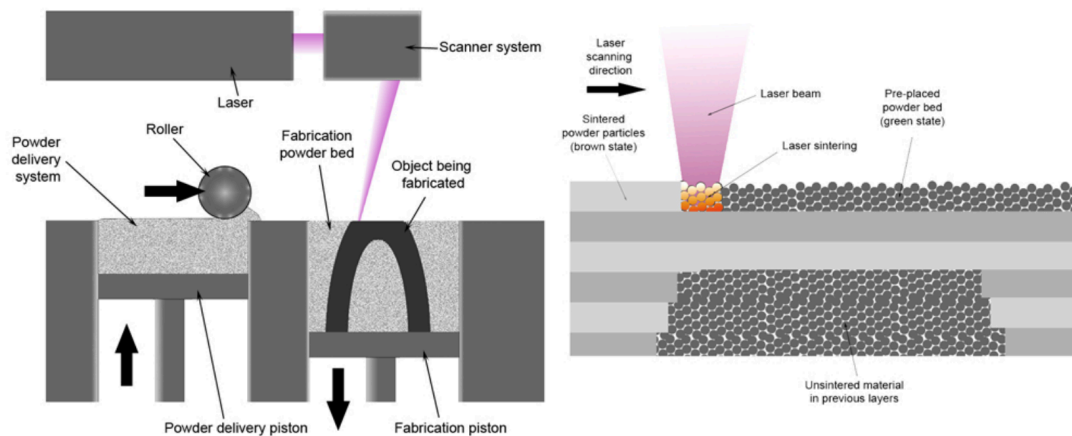

Figure 1. Selective Laser Sintering process overview (Palermo, 2013)

For the Selective Laser Sintering of plastics, a majority of machines are maintained at an elevated temperature throughout the entirety of the build. The powder bed must be preheated and then maintained well above the recrystallization temperature (T_c) of the material but just slightly below its melting temperature (T_m). This region is known as the sintering window of the material and can be seen on the next page in Figure 2. The large hump on the top indicates the T_m of the material while the dip on the bottom lines indicates the material's T_c. This graph is known as a DSC curve and will be explained in detail in following sections. Note that the sintering window shown below is for a non-specified material.
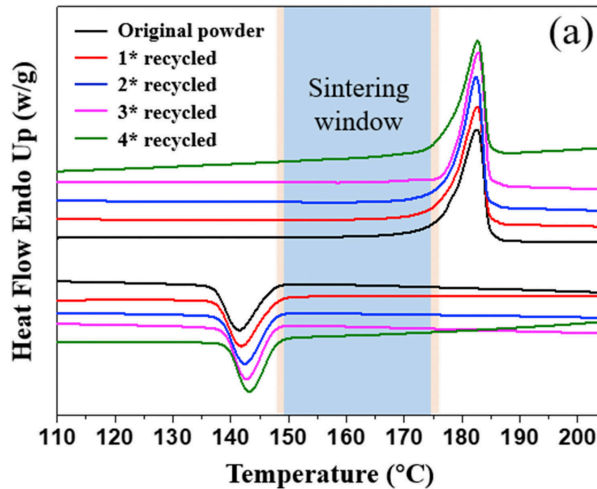
Figure 2. Sintering window of a material (Chen, et al., 2018)

Keeping the material well above the recrystallization temperature ensures that the particles do not recrystallize during the build. This allows the entire part to cool simultaneously, after every layer of the build is complete, enabling a strong bond to form between adjoining layers and reducing distortion due to thermal gradients. The preheat temperature is set just below the melting temperature of the material for several reasons. These reasons include minimizing energy input required to melt the material, prevention of curling (discussed later), and the creation of stronger parts (Wroe, Gladstone, Phillips, Fish, Beaman, & McElroy, 2016). Along with the preheat temperature of the powder bed, the laser parameters used during a build are other key aspects that significantly affect the outcome quality of an SLS build. These laser parameters, among others, include laser power, scan speed, and hatch spacing. Finely tuning these parameters and the preheat temperature is critical to preventing many potential problems in the SLS process. For example, scanning too fast or using too low of a laser power can result in partially dense parts that exhibit inferior tensile strengths, while setting the preheat temperature too low can lead to curling. Curling is when the exterior edges of a part rise up or "curl" due to excessive heat transfer and large temperature gradients between a layer and the freshly rolled powder. The raised or curled portion of the sintered part can then contact the roller or powder spreading apparatus as it spreads powder causing the parts to drag across the powder bed and ruin the build.

Parameter development for new materials in SLS is critical to the maturation of the process, not only increasing its capabilities but also making it more appealing to new industries and applications. With the ability to utilize a wider array of materials in SLS, parts that were once made by traditional manufacturing processes can now be fabricated in SLS. Carbon fiber reinforced thermoplastics are of interest as they offer strong, yet lightweight alternatives to many heavier metals. However, before a material can be built using SLS, research must be performed to establish build parameters and set points for the machine to run the desired material. This thesis specifically investigates parameter and set point development for a material novel to the SLS process, Carbon Fiber Reinforced Polyetheretherketone (CFR PEEK). Additionally, a standard procedure of parameter development for innovative SLS materials is established. Tensile bar builds are then completed and the results are compared to identify the best processing parameters. In order to compare the results of these builds, establish a best set of lasing parameters, and determine which parts from the build are considered "good" parts, criteria must

be identified. For the purpose of this study, tensile strength is used as the quantitative indicator of the quality of the fabricated part. For each build, a set of tensile tests is run to record the tensile strength of each tensile bar. This information is important as it helps to inform designers of limitations when designing parts for fabrication by SLS. The tensile strengths can also be used, along with the lasing parameters and temperature set points, to construct and fit models that allow for predicting and controlling the tensile strengths of future builds.

The second part of this thesis focuses on the correlation of the Carbon Fiber Reinforced PEEK part's thermal history (temperature throughout the sintering process) to its measured tensile strength. Constructing an accurate model allows for precise part strengths, based on the input parameters, to be confidently predicted and used to guide design without expensive testing. Previous research has already linked the average post-sintering temperature to the measured mechanical strength of the part. In general, the higher the average post-sintering temperature, the higher the mechanical strength. This correlation, however, is fairly weak and is subject to a large amount of variability. A 2016 study suggested that minimum post-sintering temperatures actually show a stronger correlation than the average post-sintering temperatures (Wroe, Gladstone, Phillips, Fish, Beaman, & McElroy, 2016). This thesis explores this topic in further depth, comparing the correlations between different measures of an SLS part's thermal history and its mechanical strength. Several different models are evaluated and a recommendation is given for future modeling of parts built using Selective Laser Sintering.

The previous discussion has introduced several topics surrounding the fabrication of Carbon Fiber Reinforced PEEK parts via Selective Laser Sintering. With that established, this thesis will accomplish three major goals:

- Develop a standard process for identifying machine set points and laser parameters for materials new to the Selective Laser Sintering Process
- Determine processing parameters for the Selective Laser Sintering of Carbon Fiber Reinforced Polyetheretherketone
- Improve correlation techniques for predicting mechanical strength of a part based on its thermal history during fabrication

Chapter 2. Process Overview for Building in Novel SLS Materials

The first goal of this thesis is the development of a standard process for identifying machine set points and build parameters for fabricating with novel materials in the SLS process. More often than not, trial and error methods are used to learn how to build with a new material (Spears & Gold, 2016). Additionally, standard parameter sets provided by a company may or may not be tailored to the maximize the desired part quality of the build. For example, one set of parameters and set points will produce a part with excellent geometrical accuracy and aesthetic appearance but relatively poor mechanical strength, while another set gives poor aesthetics and dimensional accuracy but a much higher mechanical strength. For the purpose of this thesis and parameter development for CFR PEEK, outputting parts with the maximum achievable tensile strength is desired. The steps presented in the list below are a summary of the steps taken to build in a new material. Each of these steps and their success criteria is described in further detail in the subsequent sections.

Steps for Development of Novel Material Parameters in an SLS machine
1. Verify powder particle size is suitable for Selective Laser Sintering Process
2. Identify sintering window of material
3. Use visual tests to narrow sintering window and determine powder bed preheat temperature
4. Use visual tests to identify laser powers suitable for use with selected powder bed preheat temperature
5. Identify test matrix for fabricating parts based on selected parameters
6. Run series of test builds
7. Evaluate desired quantitative metric for each build to determine best set of operating parameters

Chapter 3. Characterization of CFR PEEK Powder Properties

Section 3.1 Carbon Fiber Reinforced PEEK Material Overview

As discussed briefly in the previous section, the capability to build in new materials opens the door for applications of the SLS procedure to new industries. Carbon Fiber Reinforced PEEK is of specific interest to both the aerospace and medical fields for several of its unique material properties. The CFR PEEK powder used in this thesis is a composite comprised of a Polyetheretherketone semi-crystalline thermoplastic matrix and a 10% by weight chopped short carbon fiber reinforcement (Booth, 2013). On its own, the tan-colored PEEK retains its mechanical properties (Tensile strength near 100 MPa, Flexural Modulus 140-170 MPa, Young's Modulus 3-4 GPa) up to temperatures near 336 °C, making it great for high temperature applications. It has a relatively low thermal conductivity at .29 W/(m*K) but is both non-toxic and biocompatible. Along with these human safety characteristics, PEEK has similar mechanical properties to human bone and enamel making it an important material in the medical field for several different types of human implants (Skirbutis, Dzingute, Masiliunaite, Sulcaite, & Zilinskas, 2017).

Carbon Fibers, on the other hand, are black in appearance, cylindrical in shape, and are characterized by extremely high mechanical properties (Tensile Strength 3.5 GPa, Young's Modulus 230 GPa) (Drechsler, Heine, Medina, & Mitschang, 2016). Additionally, Carbon Fibers have a high thermal conductivity of 24.0 W/(m*K) (Joven, 2012). Rock West Composites, a supplier of CFR PEEK, indicates that the carbon fibers "improve the compressive strength, stiffness, and load carrying capacity of the PEEK" while also providing a "significantly higher thermal conductivity" (Rock West Composites, 2018). When combined into the CFR PEEK composite, the two materials create an extremely strong yet lightweight, biocompatible and chemically resistant material. This allows Carbon Fiber Reinforced PEEK to also be used in medical implants just as non-reinforced PEEK is and also used as a lightweight metal replacement for many brackets and components in the aerospace field. CFR PEEK is currently manufactured via injection molding for the majority of these applications.

Section 3.2 Scanning Electron Microscopy (SEM) Particle Size Analysis

The diameter of the particle sizes of a powder used in Selective Laser Sintering need to be within a certain dimension in order to work with a selective laser sintering machine. It is desired for the average particle diameters to be within 20 μm and 80 μm (Schmid, Amado, & Wegener, 2016). In order to quantify the particle diameter distribution of the CFR PEEK as well as the average diameter and length of the cylindrical chopped carbon fibers, a Scanning Electron Microscopy study was conducted. Scanning Electron Microscopy utilizes a Scanning Electron Microscope to inspect the surface and composition of an object. It operates by directing a focused beam of electrons over the surface of the object to be imaged. When the electrons hit and penetrate the object's surface, three things are created: secondary electrons, back scattered electrons, and X-rays. This information is then collectively used by the machine to create an image of the object, which is then displayed to the operator on the computer monitor. The main advantage of the SEM to traditional light microscopes is its extremely fine resolution. This is due to the significantly smaller wavelength of the electron when compared to light (nanoScience Instruments, 2018).

A Quanta FEG 600 SEM was used to image a sample of the CFR PEEK. Several images at varying magnifications were recorded and utilized for analysis on particle diameter of the PEEK and Carbon Fibers along with the length of the Carbon Fibers. Figure 3, shown below, is an unmodified image of the CFR PEEK powder taken with the SEM. Irregular shaped PEEK particles of varying sizes take up most of the space and both short and long, chopped carbon fibers can be seen sprinkled throughout the image. The image was taken at a magnification of 100X and a bar is provided on the bottom center of the image for scaling.
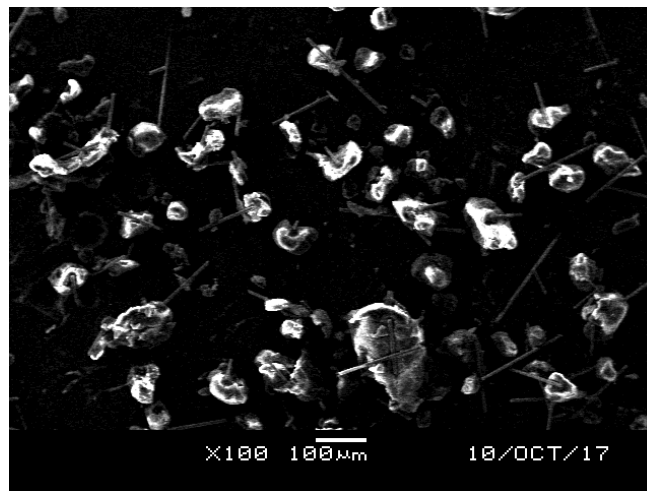

Figure 3. 100X SEM image of CFR PEEK

Once the images were recorded, image analysis was performed in order to quantify the mean particle diameter of the PEEK and the mean length and diameter of the Carbon Fibers. Although most are irregular in shape, in order to calculate the mean diameters, PEEK particles are assumed to be spherical with a circular cross section. The analysis was performed in ImageJ, an image-processing program based in the Java programming language. Although it has many uses, for the purpose of this research it is used in the analysis of the SEM images and the thermal data collected by the MWIR. With the SEM images in ImageJ, contrast adjustments were applied

to SEM images in order to isolate the PEEK particles and Carbon Fibers from the background. Cross-sectional areas of the isolated particles were then automatically recorded utilizing the capabilities of ImageJ and the diameters of the particles were calculated using the equations seen below. For these equations, A is the cross sectional area, r is the radius, and D is the diameter of the particle.

$$A = \pi r^2$$
$$r = \frac{D}{2}$$
$$D = \sqrt{\frac{4A}{\pi}}$$

After the diameters were calculated for particles from multiple images of the CFR PEEK sample and the Carbon Fiber lengths recorded, histograms were constructed to visually display both of the data sets. The Carbon Fiber diameter was very uniform at 8 µm and therefore a distribution was not necessary. The average mean particle diameter (D_{50}) of the PEEK particles was 47.8 µm for a sample size of 109, and was well within the desired diameter range previously specified for use in SLS. The average Carbon Fiber length was found to be 122.2 µm with a sample size of 67. Maximum and minimum values along with the mean and standard deviations are displayed on each of the figures below.
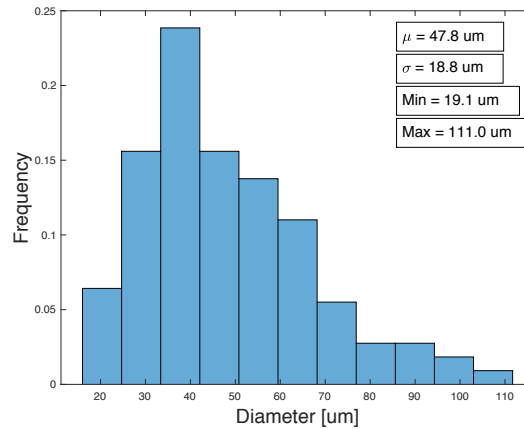
Figure 4. Mean particle diameter of PEEK particles in CFR PEEK
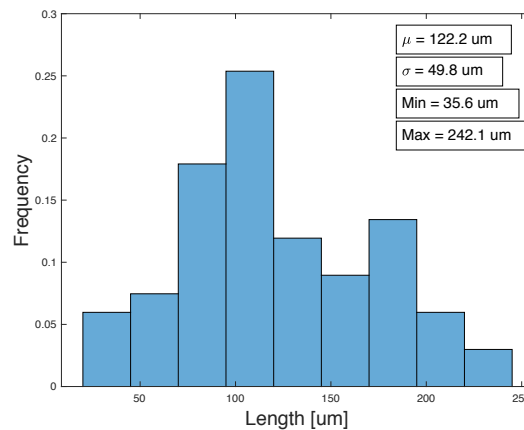
Figure 5. Length Distribution for Carbon Fiber in CFR PEEK

Section 3.3 Sintering Window Determination via Differential Scanning Calorimetry (DSC)

Once the powder was identified as having a mean diameter suitable for use in Selective Laser Sintering, it was then necessary to determine the sintering window for the CFR PEEK. In order to identify this window a Differential Scanning Calorimetry (DSC) test was run. In a DSC test, the material to be tested is placed in a pan on a heating element and an identical reference pan is placed on a separate heating element. The two pans are then increased in temperature at a constant rate. It takes a different amount of heat to increase the temperature of both pans at the same rate due to the sample material in one of the pans. The measured difference in heat output necessary to keep the two pans at the same temperature, which is equivalent to the amount of heat going into the test material, can then be recorded and plotted as a function of temperature. This chart is referred to as the DSC plot. The heat capacity of the material being tested can then be calculated by dividing the heat input to the material by the temperature increase of the material. Upon heating of the material, eventually the melting temperature will be reached. The material will then begin the endothermic melting process and additional heat output by the heater is required to maintain a constant temperature increase. This shows up as a large increase in heat output on the DSC plot, identifying the melting temperature of the material. Once the melting process is finished, the pans and material will be reduced in temperature at the same constant rate. Just above the recrystallization temperature, the polymer being tested will begin to change into a crystalline formation, giving off heat in the process. This exothermic process will show up on the DSC plot as a decrease in heat output by the heater because it is now required to put out less heat to maintain the same temperature. This is how the recrystallization temperature of the material is determined (Polymer Science Learning Center, 2018).

Shown below in Figure 6 is the recorded DSC plot from the test. The heat flow is recorded on the Y-axis in -W/g while temperature is recorded on the X-axis in °C. Note that the Y-axis is recorded in negative units (measuring heat output by heater) causing decreased heat output (recrystallization) to be a bump and increased heat input (melting) to be a dip on this particular DSC plot. Although hard to read due to the output image from the instrument, the first bump and the first dip on the graph are the important things to focus on. The first bump, identifying the recrystallization temperature of the sample, occurs at approximately 320 °C. The first dip occurs at approximately 371 °C and indicates the melting temperature of the sample. Additionally, there is a third dip on the chart resulting from errors when switching from the heating to the cooling cycle that should be ignored for the purposes of this thesis.
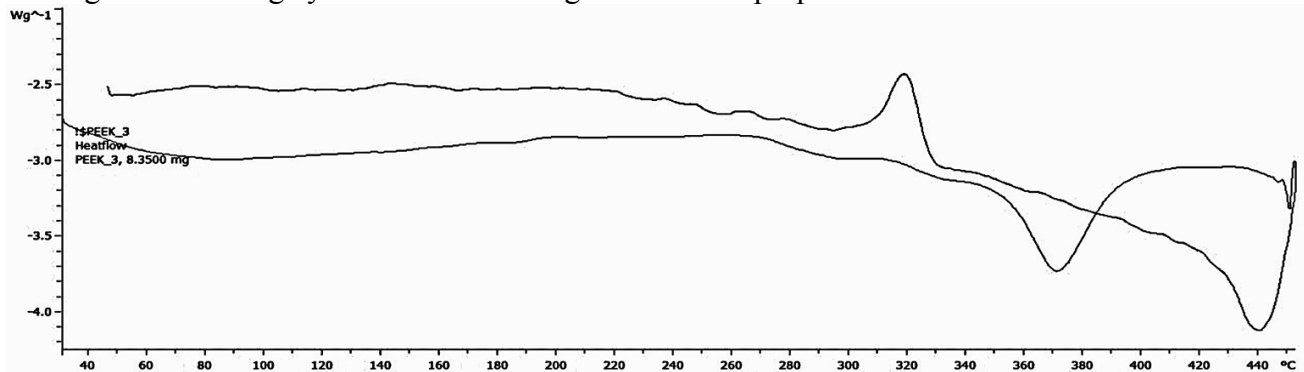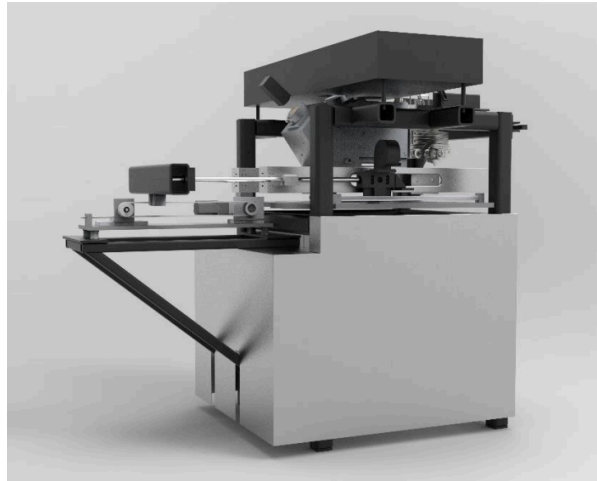

Figure 6. DSC curve for CFR PEEK

# Chapter 4. Experimental Set-Up for Laser Parameter Determination

Section 4.1 LAMPS Machine Overview

**Figure 7. LAMPS machine CAD rendering**

All of the builds required for the completion of this thesis were executed on the Laser Additive Manufacturing Pilot System (LAMPS) at the University of Texas at Austin, shown above in Figure 7. LAMPS is a custom designed machine built with the intention of being the most instrumented and adjustable Selective Laser Sintering apparatus in the world. LAMPS is equipped with three cameras that are used to monitor the powder bed in real time, collect and record the thermal history of the powder bed for the entirety of each build, and provide feedback control to several heating elements. The three monitoring cameras include an Edmund Optic Monochrome USB visual camera with a 25 Hz frame rate (Edmund Optics Inc., 2018), a FLIR A6701 MWIR camera with a stationary reference frame and a 60 Hz frame rate (FLIR, 2018) and a bore-sighted FLIR SC8240 MWIR camera with a 2.24 kHz frame rate (FLIR Systems, 2013). The camera locations are designated in the cross section view of the LAMPS machine on the next page in Figure 8. Note the SC8240 MWIR camera was not used during the completion of this thesis. Furthermore, LAMPS is equipped with more than 40 strip heaters and 3 quartz lamps used to heat the atmosphere of the main chamber as well as the powder bed. The quartz lamps offer precision control of the powder bed temperature and are controlled by PID feedback from the MWIR stationary camera. Each of the 40 strip heaters has an attached thermocouple that is used for temperature control by PID feedback as well. All of the cameras and feedback control is run by a custom LabView software program developed specifically for the LAMPS machine.
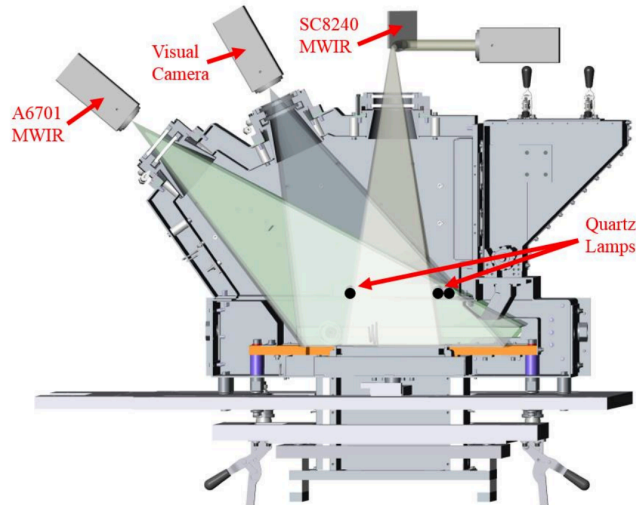
Figure 8. LAMPS machine camera locations

A black laser box, seen in Figure 7, is mounted to the top of the LAMPS machine and houses all of the optical components used to control the 40 Watt CO_2 laser used in the sintering process. A set of mirrors directs the laser into the optical track where a series of lenses collimates and then focuses the laser onto the galvanometers. The galvanometers are then used to control the laser's position for sintering the powder bed. Although the laser is rated for 40W, full power output is not achieved when used by the LAMPS machine. Power is lost due to multiple Zinc Selenide windows in the optical track along with contamination on the window leading into the build chamber. A laser power curve was measured before using the laser in the CFR PEEK experiments and the results can be seen below in Figure 9. Laser Power command given as an input to the LAMPS software is on the X-axis as a percentage while output Laser Power is on the Y-axis in Watts. A trend line was fitted to the data and its equation and R^2 value are displayed on the chart. The maximum laser power output was measured to be 17.3 W at a command of 100% power.
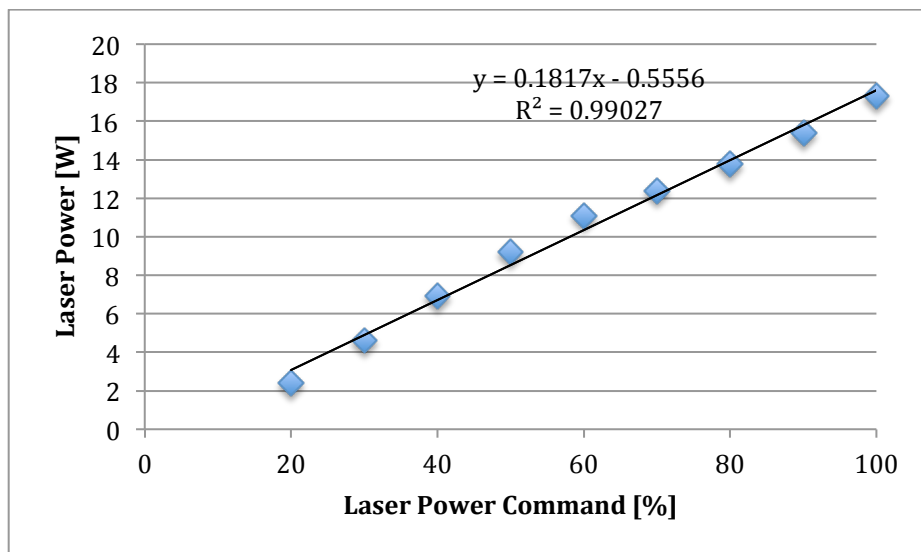
Figure 9. Laser Power Curve

Section 4.2 Visual Sintering Tests for Powder Bed Preheat Temperature Determination

The sintering window determined earlier from the DSC (320 °C to 371 °C) provides a starting point for identifying the set points and parameters for building in CFR PEEK. The majority of the sintering window, however, would not actually work for building. At lower temperatures, curling would occur leading to failed builds while at higher temperatures near the melting point, the entire powder bed may sinter together as CFR PEEK is a highly thermally sensitive material. In order to identify these problem areas and determine the best range for building in CFR PEEK, powder spreading and visual sintering tests were performed.

Roller spreading tests are first performed to determine a powder drop set point. In the LAMPS machine, powder is dropped from a hopper onto a stainless steel plate. A quartz lamp then preheats the powder so it will easily spread into a uniform, defect free layer. These tests are relatively quick as a wide range of temperatures give a sufficient powder drop preheat and a uniform powder bed. For the CFR PEEK, a set point of 330 °C was identified from rolling tests. An example of a smooth, defect-free powder bed created at 330 °C can be seen around the sintered objects on the top image in Figure 10. Note that the darker area seen on the right hand side of both images is a shadow caused by debris on the visual camera window.
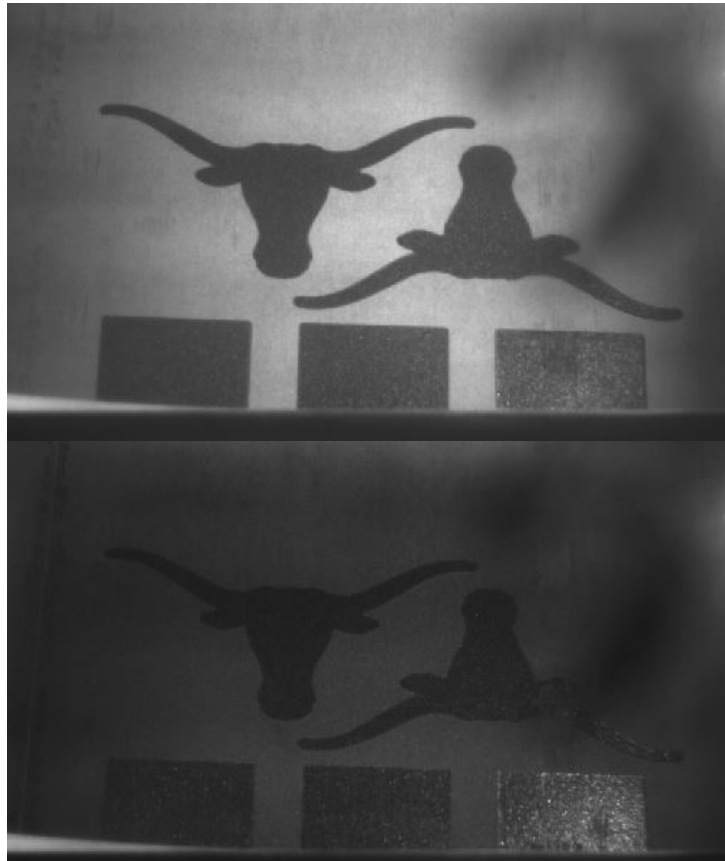

Figure 10. Smooth powder bed (Top) vs. Overheated powder bed (Bottom)

As mentioned earlier, the quartz lamps control the powder bed temperature via PID feedback from the MWIR stationary camera. Sintering tests were started at a quartz lamp set point of 360 °C, as anything below that caused curling issues on the exterior edges of the parts.

However, the main problem that occurred with the CFR PEEK was the complete sintering of the powder bed at higher temperatures. The CFR PEEK is thermally sensitive and a large flash of the quartz lamp would cause the powder bed to turn a dark gray and sinter together. This can be seen in the bottom image of Figure 10. The CFR PEEK was heated too much and melted, giving it the very dark gray appearance under the same lighting conditions as the image above it. When this occurs the build is deemed failed and blank layers must be deposited on top to start over or the build must be cancelled.

Several rounds of sintering individual layers at a fixed laser power of 7.6 Watts were performed at quartz lamp set points ranging from 360 °C to 370 °C in increments of 2 °C. The highest set point of 370°C resulted in the sintering of the entire powder as shown in Figure 10. It is desired to pick the highest set point possible that doesn't sinter the powder bed together as previous research has linked higher temperatures to stronger parts achieved by a full melting of the material (Wroe, Gladstone, Phillips, Fish, Beaman, & McElroy, 2016). Figure 11 shown below, with both images under the same lighting conditions, shows the difference between the sintering quality for the set points of 362 °C (top image) and 368 °C (bottom image). The darker gray powder bed on the bottom image indicates a higher temperature. The higher set point gave a much darker sinter at this laser power, indicating that a higher level of melting was achieved. The visual sintering tests identified a powder bed preheat temperature of both 366 °C and 368 °C to use for the tensile bar builds of the study. However, the crosses sintered at these set points with only 7.6 Watts from the laser still did not show signs of complete melting. The next step was sintering tests to identify laser power levels for use with these determined set points.
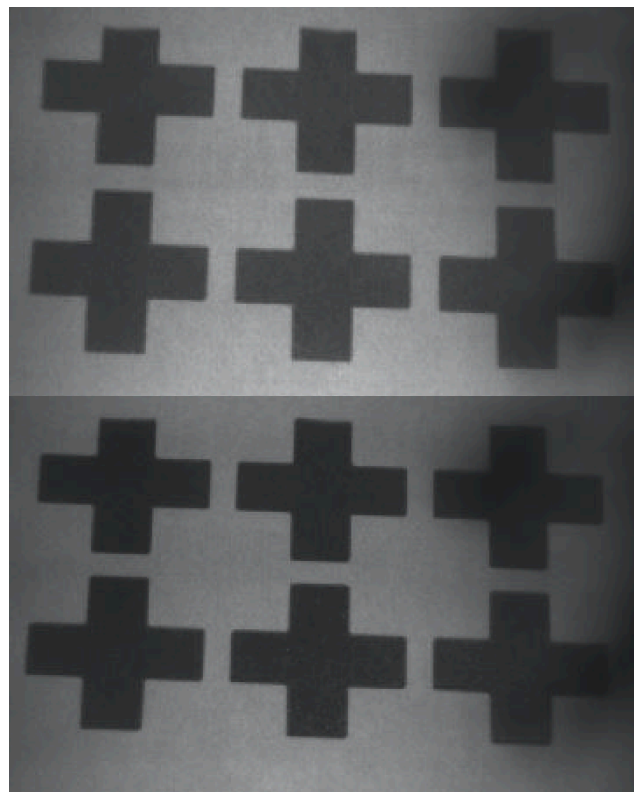
Figure 11. Sintering quality comparison for 362 °C (Top) and 368 °C (Bottom)

Section 4.3 Visual Sintering Tests for Laser Build Parameter Determination

With powder bed preheat temperatures selected for the tensile bar builds, laser settings needed to be established for the tensile bar builds. Table 1 below shows the fixed laser settings that were used for all of the builds and sintering tests. These parameters are standard values used in the LAMPS machine based on previous sintering experimentation.

Table 1. Standard laser parameters

Scan Speed	Jump Speed	Scan Delay	Jump Delay	Hatch Spacing	Laser On/Off Delay
1500 mm/s	1500 mm/s	1500 mm/s	700 mm/s	300 um	900 us

Laser powers in increments of 10% (1.81 W) ranging from 45% of full power (7.62 W) up to 95% of full power (16.71 W) were tested at the preheat temperature of 366 °C. The images in Figure 12 below show the difference between three different laser powers of 45% (7.62 W on Top L), 75% (13.07 W on Top R), and 95% (16.71 W on Bottom). 45% is included for reference with the two best settings (75% and 95%) shown for comparison.
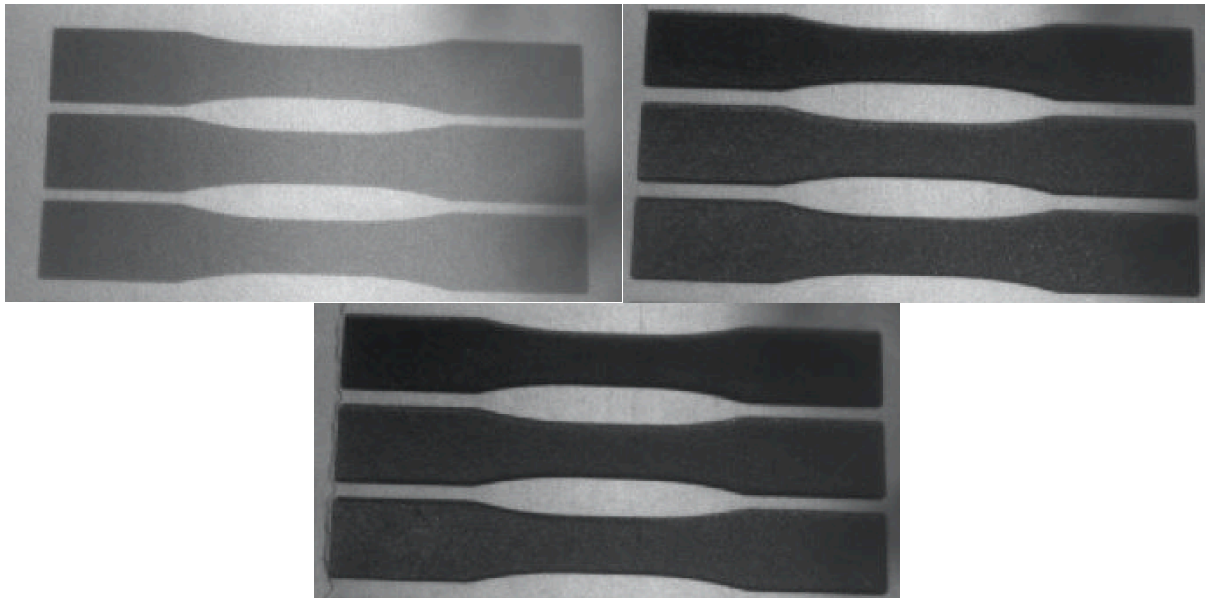
Figure 12. Sintering quality comparison for 7.62 W (Top L), 13.07 W (Top R), and 16.71 W (Bottom)

Several indicators were used throughout the sintering tests in order to qualitatively distinguish between the different laser powers. The two main things that were being inspected were the color of the sintering and the depth. Previous experimentation with the CFR PEEK has shown that the originally gray powder turns a dark gray and eventually black when enough energy is deposited. The darker color is an indicator of achieving full melting of the material while a light gray is indicative of only partial or weak sintering. Additionally, when good melting has been achieved the part can visually be seen to have sunken into the powder bed. Close inspection of the part's edges will show a lip, indicating melting has occurred.

Both the 75% and 95% laser power have a dark gray, almost black color, showing that a close to full melting is being achieved. This is a stark contrast when compared to the lightly sintered gray color seen with 45%. Additionally, a close look at the bottom two images of Figure 12 reveals the parts have sunken down below the powder bed upon sintering. This is a great indicator that melting was achieved. This is not seen on the 45% image. The 95% laser power managed a slightly deeper melt than the 75% laser power, however, both were selected to test in the tensile bar builds. It is also important to note that it is possible to degrade the powder by putting too much energy into it. This is usually characterized by a loss of the ability to resolve smaller features. In the tensile bars, rounded corners would be seen if the laser power were too high. The corners in the bottom image of Figure 12 do not appear to be more rounded indicating this laser power is not too high and an even higher wattage could potentially be used in the future.

Section 4.4 Tensile Bar Build Details and Build Matrix

The previous chapters and sections described the process for powder characterization to determine the sintering window as well as how visual tests were used to confirm valid powder bed preheat temperatures and laser settings for building in CFR PEEK. Using this information a build matrix was established to be able to quantify tensile strength for bars at a range of temperatures and parameters. Two powder bed preheat temperatures of 366 °C and 368 °C along with two laser powers of 75% (13.07 W) and 95% (16.71 W) were used for a total of four different combinations. The four builds can be below in Table 2.

Table 2. Build matrix

Build #	Quartz Lamp Set Point (°C)	Laser Power (W)
1	366	13.07
2	368	13.07
3	366	16.71
4	368	16.71

Each of the builds listed in Table 2 consisted of a total of nine shortened ASTM D638 Type I tensile bars. The tensile bar grips were slightly reduced and the length of the gauge section was decreased in order to keep the tensile bars more towards the center of the LAMPS build box. When full size ASTM Type I tensile bars were test sintered the far edges curled as the temperature was too cool on the far sides of the build box. Nine tensile bars were chosen due to the current limitations of the LAMPS machine. One of the quartz lamp currently cuts directly across the MWIR stationary camera's view of the powder bed causing half of the powder bed to be blocked out. This means the thermal history cannot be recorded by the MWIR and post-analysis cannot be completed. Therefore, only three bars fit in the powder bed that can be seen by the MWIR stationary camera.

Three sets of the tensile bars were stacked on top of each other with 15 blank layers in-between each set. The 15 layers allowed the powder bed to come back to the preheat temperature before the next layer of tensile bars were fabricated. The bars are branded with numbers and shapes for identification purposes during breakout and post-build analysis.
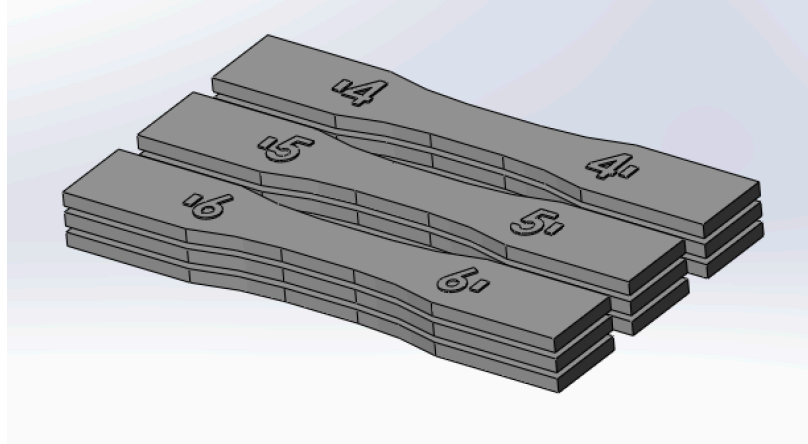

Figure 13. CAD model of full tensile bar build

Chapter 5. Post Build Analysis for Tensile Strength Quantification

Section 5.1 Tensile Testing Results

After the series of four builds had been run, the tensile bars were tensile tested according to ASTM 638 methodology using an Instron 3345 5 kN tensile testing machine. The force at failure was recorded for each of the individual bars. After measuring the cross-sectional area for each bar stress at failure was calculated and recorded as the tensile strength. The stress equation below where σ is stress (tensile strength), F is force and A is cross sectional area was used to calculate tensile strength.

$$\sigma = \frac{F}{A}$$

Additionally, a box plot showing the tensile strength data for each individual build was created in order to visually compare the effects that parameters had on output tensile strength. This plot is shown on the next page in Figure 14.
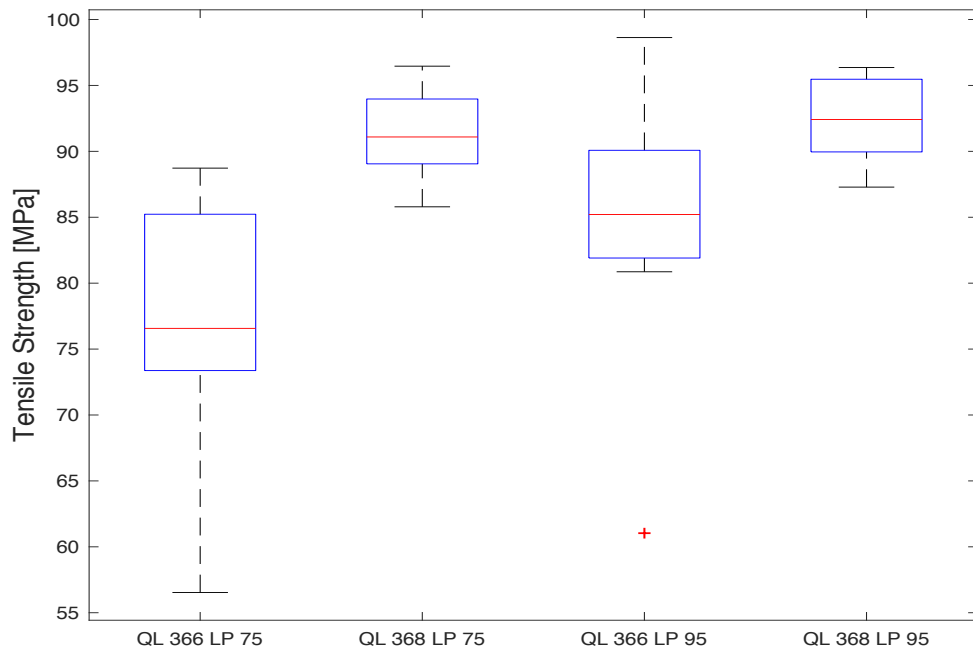
Figure 14. Tensile Strength summary for completed build matrix

In Figure 14, tensile strength is on the Y-axis measured in MPa while the bottom axis identifies the build parameters. "QL" is short for quartz lamps and identifies a set point of either 366 °C or 368 °C. "LP" is short for laser power and is set to either 75% (13.07 W) laser power or 95% (16.71 W) laser power. The builds are labeled 1-4 as identified on the X-axis. The strongest tensile bar built was in build 3 at a tensile strength of 98.6 MPa while the highest tensile strength average was 92.5 MPa for build 4. A look at the difference between the quartz lamps set points of 366 °C and 368 °C shows a significant increase in tensile strength as the temperature is increased at both laser power settings. Additionally, at 366 °C a large increase in tensile strength was seen as the laser power was increased, but only a slight increase at 368 °C. It is also important to note the amount of variance in tensile strength at a quartz lamp set point of 366 °C when compared to 368 °C. The higher set point made builds with a lot less variance and no statistical outliers. Due to the significantly reduced variance, most likely a result of achieving full melting in all of the bars, as well as higher average tensile strengths, a 368 °C set point was deemed better for building in CFR PEEK. Furthermore, at 368 °C the 95% laser power gave a higher average tensile strength than the 75% laser power. However, the increase in tensile strength was not significantly different and further testing should be ensued to confirm. In conclusion, a set point of 368 °C should be used with a laser power of 95% for currently building in CFR PEEK. It is important to note for different criteria, such as accounting for dimensional accuracy, other parameter sets may have been chosen as the best parameters. For this thesis, tensile strength is the only indicator used when comparing the quality of the builds.

Figure 14 establishes the overall trends seen from the build and supports previous research findings that an increase in post-sintering temperature leads to an increase in tensile strength while an increase in laser power has the same affect. With qualitative trends and best

parameters for building in CFR PEEK established, the thermal history of each tensile bar was investigated to develop better methods for correlating this thermal history with output mechanical strength.

Section 5.2 Tensile Bar Thermal History Analysis Methods using ImageJ

The optimal scenario for monitoring the thermal history in the powder bed of a build is significantly different than what was actually attainable. In an ideal scenario it is desired to have in-situ monitoring for each individual particle of every layer. Bond formations between particles could then be closely watched and defects detected as they formed in the layers. However, currently there are no methods for monitoring bond formations or ways to quantify their strength during a build. Therefore, temperature must be used as an indicator of the bond strength between particles. Using temperature, it would be ideal to have the entire temperature history for each individual particle over the course of an entire build. This is not possible either as the camera only has the ability to resolve individual camera pixels, which each contain a cluster of particles. The next best thing would be to have the entire temperature history for every pixel. Each pixel, or cluster of particles, goes through a temperature change as the laser scans across it and then moves away. The temperature profile for an individual pixel can be seen below in Figure 15.
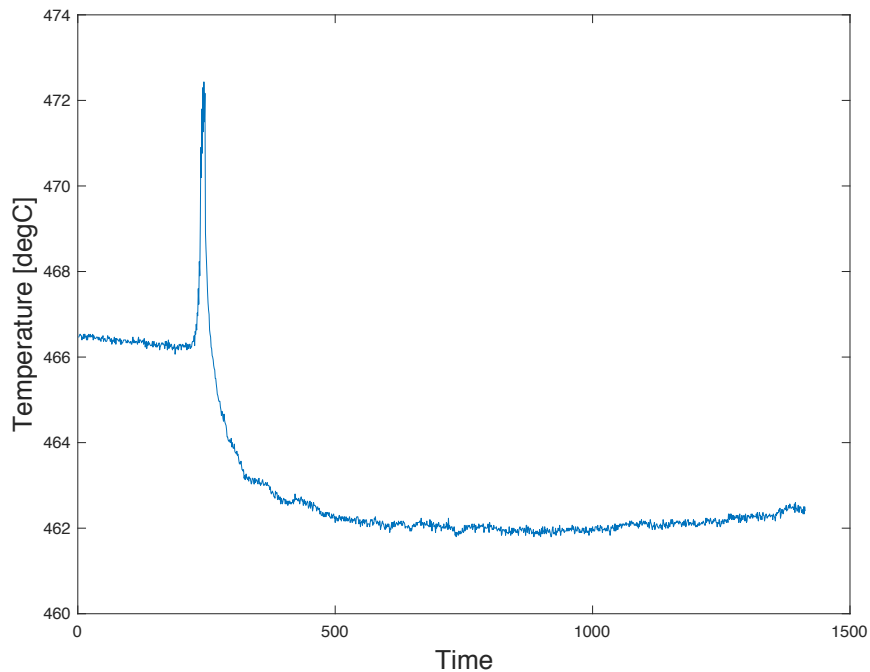

Figure 15. Temperature vs. time plot for an individual pixel

Figure 15 shows as the laser approaches the temperature rises until a max temperature is reached when the laser is directly over the pixel. After the spike occurs and the laser leaves, the temperature drops lower than it was before the laser pass. The energy input by the laser to the powder causes melting to occur. With melting comes a change in the emissivity of the powder as viewed by the MWIR camera. This results in the lower temperature reading seen in the graph.

It would be ideal to be able to record this entire curve for every pixel for each layer of a build, however, due to the MWIR stationary camera frame rate of 60 Hz, it is only possible to capture data points along this curve for each pixel and not the entire thing. A MWIR camera with a higher frame rate could be used, however, this is more expensive and requires large amounts of data storage. Developing accurate approximation techniques with slower frame rates can decrease analysis times, required data storage, and associated costs. Moving forward with knowledge of the collected data's limitations, methods must be developed for approximating accurate temperature histories and subsequently correlating them with the mechanical strengths of the produced parts.

Temperature analysis methods in previous research have used use the post-sintering temperature as a way of quantifying temperature data and correlating it to mechanical strength for a part built via SLS. For means of comparison, initial temperature analysis of the tensile bars built in CFR PEEK were performed using this method, (Method 1). The images used for this analysis method are each called a max composite image. The LAMPS LabView software automatically compiles the max temperature value achieved at each pixel over the course of a single layer into this max composite image. This is in attempt to capture the temperature for each pixel when the laser is directly over it, as this maximum achieved temperature is a strong indicator of bond quality and can indicate if full melting was achieved. The post-sintering temperature is simply the average value of the interior of the tensile bar on the max composite image. It is important to note that these max composite images record max temperature values when the material is melted, therefore, the temperature values used in the analysis portion of this thesis are significantly higher than the actual melting temperature of the material. The max composite image for each layer are organized into a stack with all of the layers of a build and are pulled into ImageJ for analysis. Figure 16 below shows one of the max composite images generated by the LAMPS program in the ImageJ software.
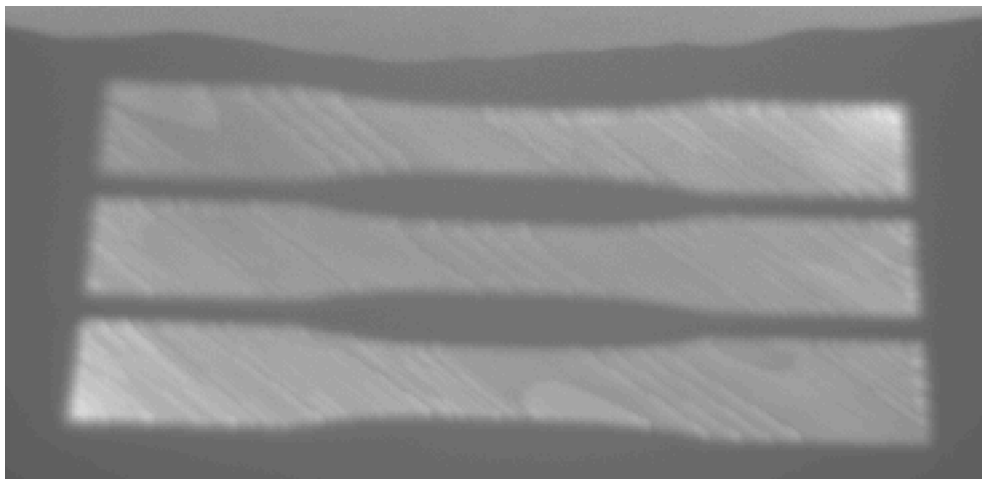
Figure 16. Max composite image of CFR PEEK tensile bar in ImageJ

For each tensile bar, a stack of the max composite images was created and imported into ImageJ. Using the Z-project function in ImageJ, the stacks of the max composite images (30 layers correspond to one tensile bar) can be turned into a single composite image that averages the value at each pixel over the entirety of the build. An ROI (Region of Interest) was then drawn

over the interior of the bar and the average taken in order to calculate the post-sintering temperature. The ROI was chosen to cover the entire bar instead of only the gauge section as failures have occurred outside this region in previous tensile tests. The subsequent section shows the correlation between this post-sintering temperature and the tensile testing results for the CFR PEEK tensile bars.

Section 5.3 Mechanical Strength Correlation with Post-Sintering Temperature

Figure 17 below graphs every tensile bar's measured tensile strength (Y-axis in units of MPa) as a function of its average post-sintering temperature (X-axis in units of °C). All four completed builds are presented together in this graph. A red trend line shows the overall trend of the data. The computed R^2 value for this trend line is .213. The graph shows an overall trend of increasing tensile strength as the average post-sintering temperature increases but the data points are fairly scattered and do not correlate well with the calculated trend line.
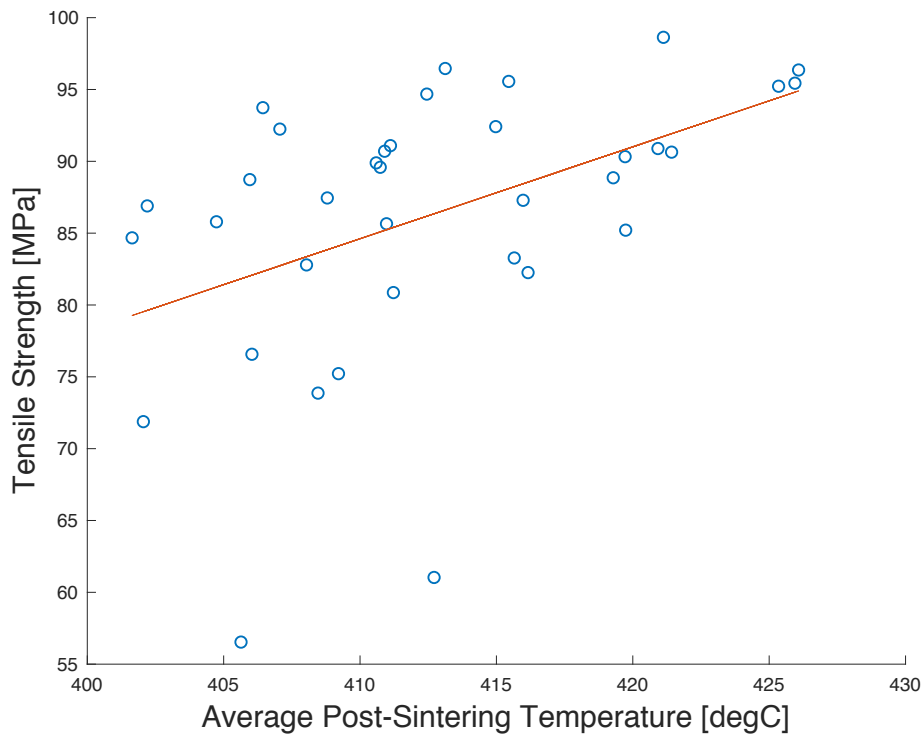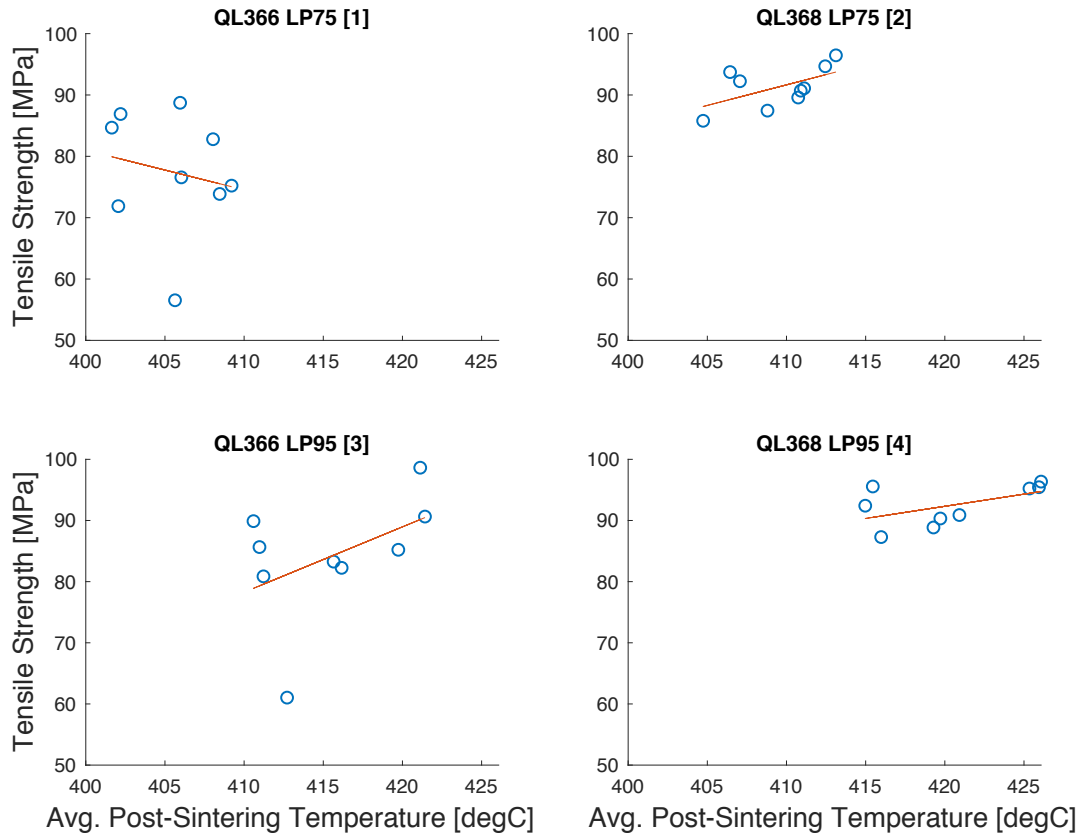

Figure 17. Tensile Strength as a function of the Average Post-Sintering Temperature for all CFR PEEK tensile bars

In this paper, R^2 values are used as a quantitative way to compare different methods of correlating mechanical strength to the collected thermal data that are explored in this thesis. It is a measure of both the closeness of the data to the trend line or model and how much variation the fitted linear model describes (Stone, Scibilia, Pammer, Steele, & Keller, 2013). The R^2 value for the graph above is low (.213) and shows that the average post-sintering temperature does not adequately correlate with strength. In order to further explore this method, Figure 18 depicts the data collected for the individual builds.

Figure 18. Tensile Strength as a function of the Average Post-Sintering Temperature for individual CFR PEEK tensile bar builds

The R^2 values for the individual builds were low as well, providing further evidence that the post-sintering temperature correlation methods are not adequate. The corresponding R^2 values in order from builds 1-4 (labeled in Figure 21) are .03570, .3198, .2123, and .2921. The current linear fit based on average post-sintering temperatures accounts for a low percentage of the variation seen in the builds. It provides no confidence that tensile strengths predicted based on the collected thermal data will be accurate. It is for this reason that the third objective of this thesis is to find better thermal correlation techniques than this average post-sintering method for more accurately predicting output tensile strengths based on thermal history data.

Chapter 6. Techniques for Improved Tensile Strength Correlations

Section 6.1 Minimum Post-Sintering Temperature Correlations

The previous figures show the average post-sintering temperature method does not accurately model the mechanical strengths being recorded for Selective Laser Sintering builds. This confirms research performed previously by Wroe et al., which concluded the average post-sintering temperatures gave low correlation coefficients with mechanical strength as well. This group then investigated measures of minimum post-sintering temperatures as a different option for correlating with mechanical strength. Significantly higher correlations were found when

using this minimum measure (Wroe, Gladstone, Phillips, Fish, Beaman, & McElroy, 2016). This idea follows the basis that a tensile bar is most likely to fail at its weakest point, or the region of the bar where the lowest temperature was achieved. Therefore, by looking at the minimum sintering temperature of a bar, instead of the average temperature, a much stronger correlation with the mechanical stress at failure (tensile strength) could potentially be found. Stemming from this idea, two separate methods were developed and tested in an effort to improve current mechanical strength and post-sintering temperature correlation methods.

Section 6.2 Absolute Minimum Post-Sintering Temperature Correlation with Mechanical Strength

The second method to be explored in this thesis involved correlating with the lowest recorded pixel temperature of the max composite image for each bar over the entirety of the build, or the absolute minimum post-sintering temperature (Method 2). This stems straight from the idea that this pixel represents the weakest area of the bar and would strongly correlate with its strength at failure. To do this, the max composite image (In attempt to record the temperature at each point as the laser passes) saved by the LAMPS software was brought into ImageJ. The Z-project command was then used to compile the lowest temperature for each pixel over the entire build into a single image. A minimum command in Matlab could then be used to find the absolute minimum temperature recorded for each individual tensile bar.
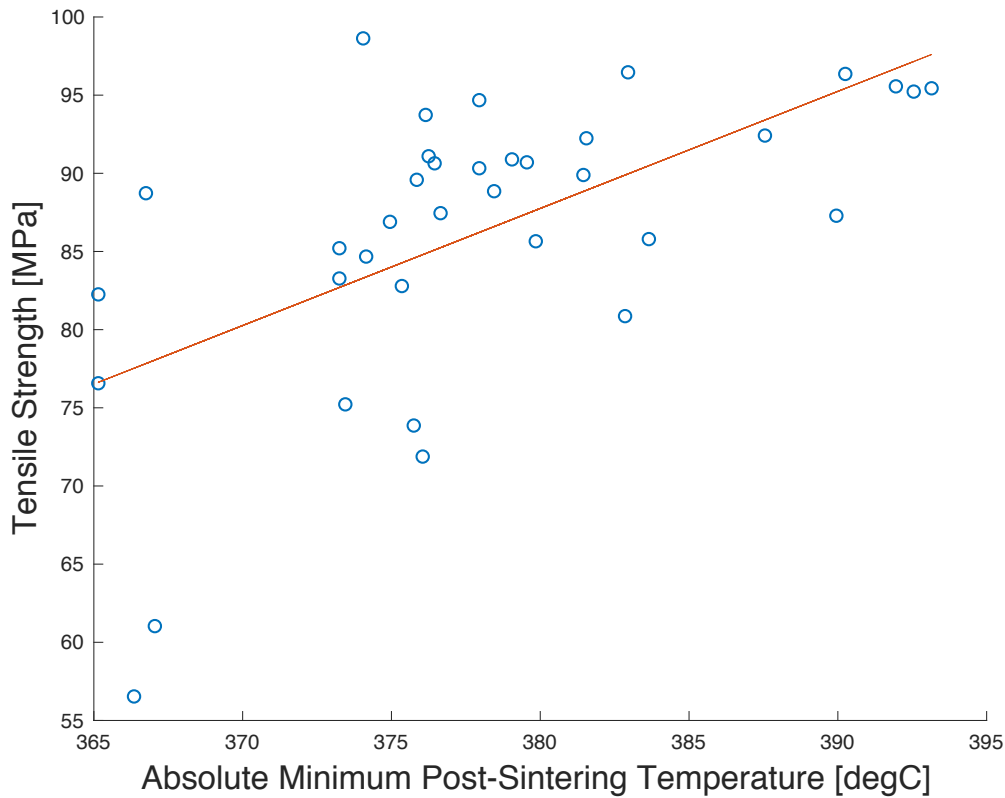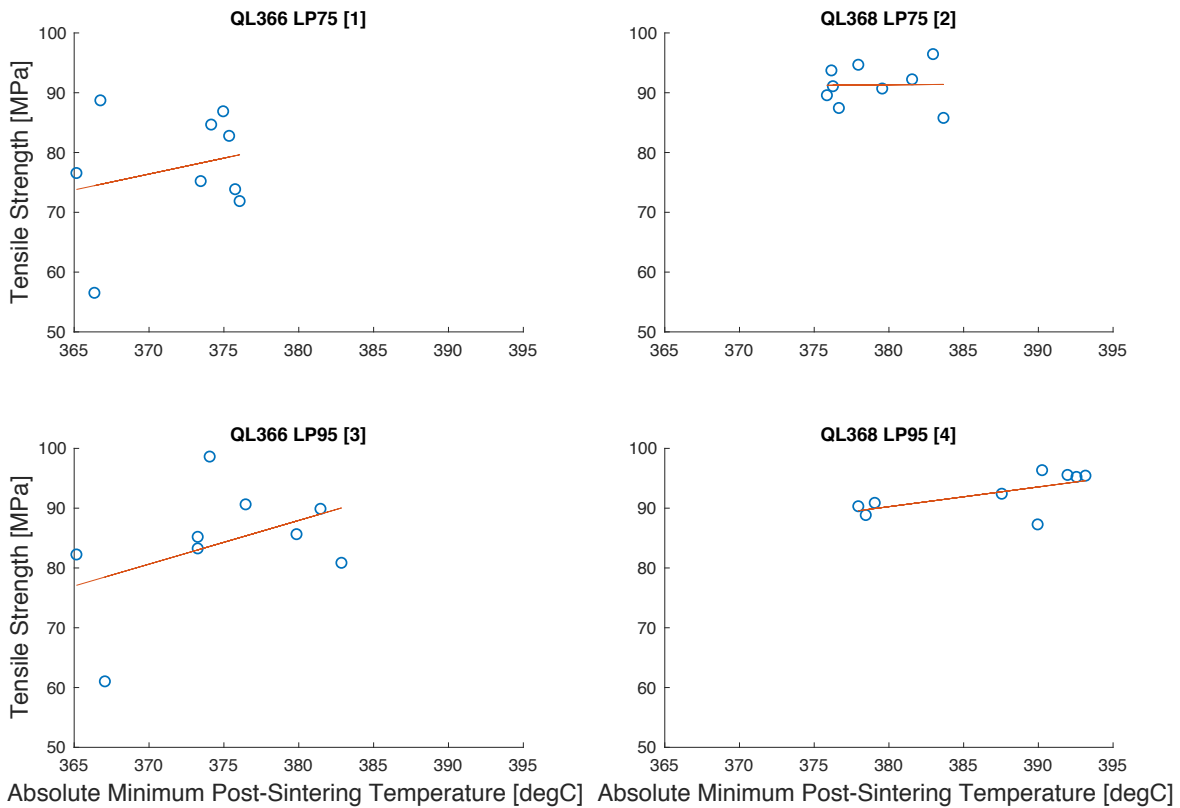

Figure 19. Tensile Strength as a function of the Absolute Minimum Post-Sintering Temperature for all CFR PEEK tensile bars

Figure 19 shows tensile strength graphed as a function of the minimum post-sintering temperature for each tensile bar. Visually, a tighter collection of data points can be seen located near the trend line when compared to the previous method. Quantitatively, the R^2 value is also higher at .3563. Below, Figure 20 shows the results from the individual builds with the new correlation method. For these builds poor correlations can be seen for the majority of the builds, however, build 4 had a much higher R^2 value. This is encouraging as build 4 was identified as the best current build parameters for building in CFR PEEK. The R^2 values for builds 1-4 with the absolute minimum sintering temperature were .0591, .0003, .1889 and .4088 respectively. Overall, for the individual builds, this method showed even weaker correlations than the post-sintering temperature methods, with the exception of build 4.
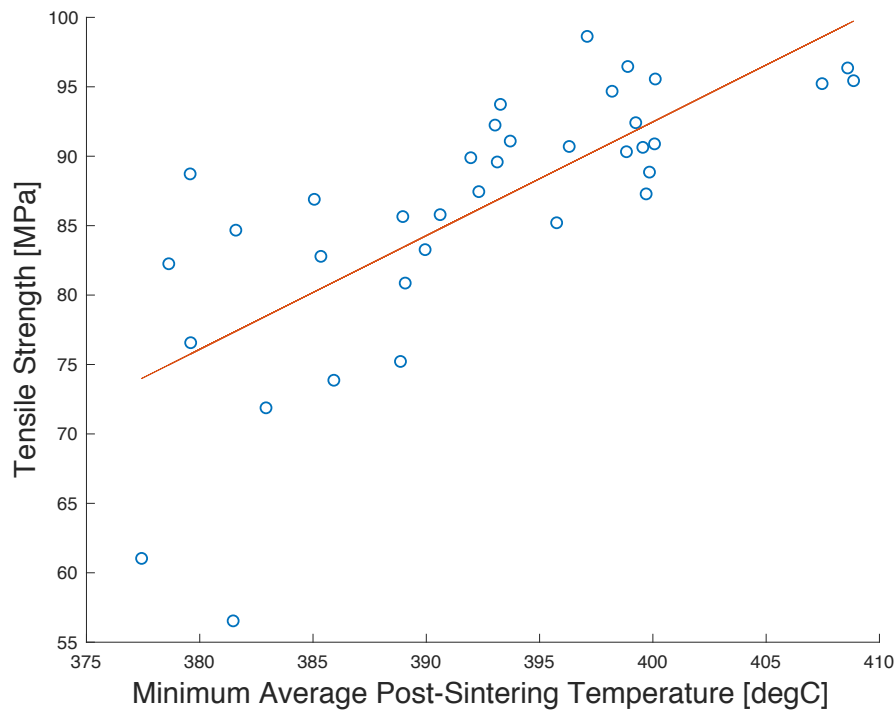
Figure 20. Tensile Strength as a function of the Absolute Minimum Post-Sintering Temperature for individual CFR PEEK tensile bar builds

A discussion is necessary for the potential downfalls of this absolute minimum measurement. By using this measurement, it is possible that the minimum values being used are actually anomalies. The minimum value taken from the minimum of all layers makes a single measurement from one layer represent an entire build. It could be that particle happened to be imaged one time while the laser was extremely far away and it therefore does not accurately represent the minimum temperature achieved of the bar during melting. One option to fix this is to run a statistical analysis and eliminate these outliers before taking the absolute minimum value. Another option is to take the average value for every pixel throughout the entirety of the build and then use the minimum value from that collection of data. This way the minimum

temperature location averaged over the whole build is identified and used, not just a single pixel measurement from a single layer. This method is explored in the next section of this thesis.
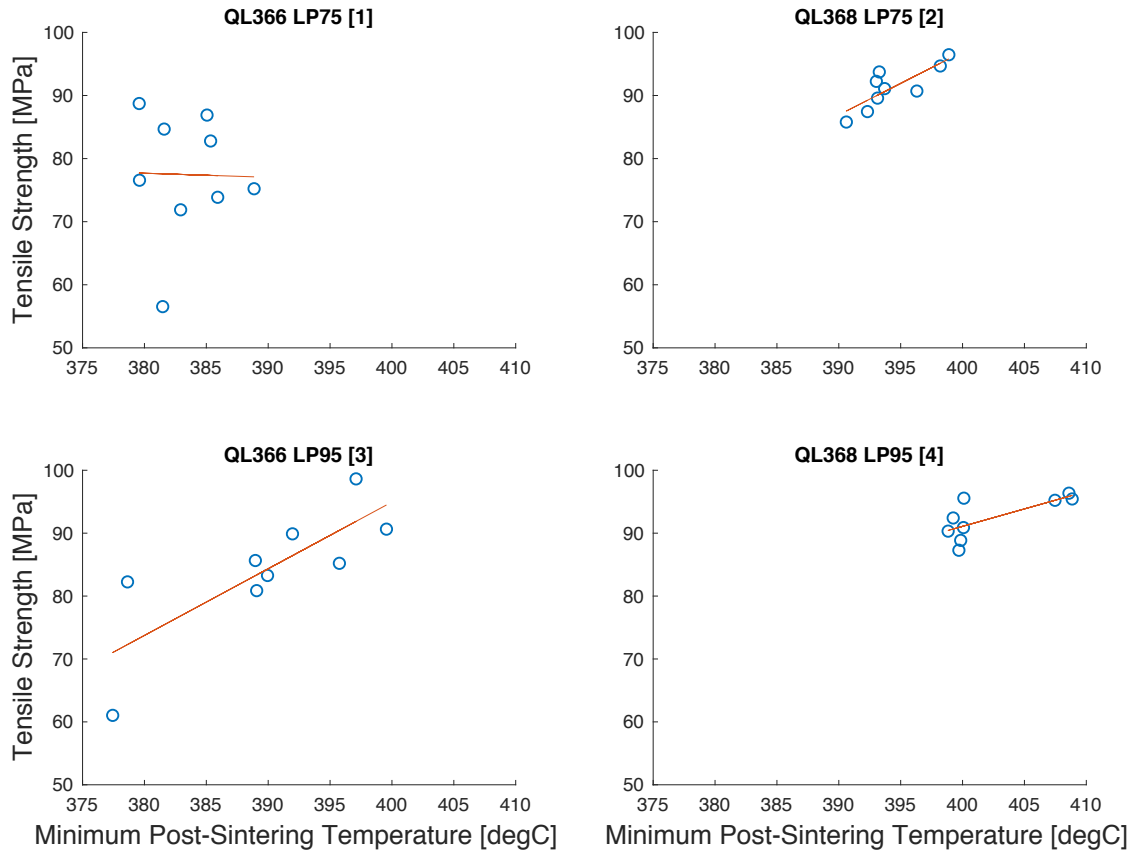
Section 6.3 Average Minimum Post-Sintering Temperature Correlation with Mechanical Strength

The final method quantified in this thesis is the average minimum post-sintering temperature (Method 3). This analysis was performed using ImageJ software as well. Z-project was used to average the value at each individual particle over the entire build. Then in Matlab, a minimum value was taken from this. Using this method, the lowest average pixel temperature over the whole build is used to represent the bar's post-sintering temperature. Averaging across the entire build eliminates the possibility of a single outlier data point being used to represent the temperature of the tensile bar.

Figure 21. Tensile Strength as a function of the Minimum Average Post-Sintering Temperature for all CFR PEEK tensile bars

Figure 21 plots tensile strength in MPa versus the minimum average post-sintering temperature in °C. The chart shows an even spread of data points scattered on both sides of the trend line. An R^2 value of .5409 makes it the model that most accurately describes the variation seen in the tensile strength data. This is a 254% increase in R^2 value when compared to the post-sintering temperature method explored earlier. The individual builds show a better correlation with the data as well and can be seen plotted in Figure 22 on the next page.

Figure 22. Tensile Strength as a function of the Minimum Average Post-Sintering Temperature for individual CFR PEEK tensile bar builds

The individual builds have corresponding R^2 values of .0004, .6635, .6277, and .5344. These R^2 values are significantly higher, especially when compared to the post-sintering temperature methods, and begin to model and explain a significant amount of the variations seen in the data. The first build had extremely low R^2 values for all of the methods that were used. These bars were likely not completely sintered due to the low preheat set point and lower laser power, potentially causing large amounts of additional variations. Several tight clusters of tensile strengths exist in the two builds identified as good laser parameters for CFR PEEK, builds 2 and 4. This shows some consistency between thermal data and output tensile strength. This level of repeatability, but to an even further extent, is what is desired in order to be able to reliably predict mechanical strengths based on measured thermal data during a Selective Laser Sintering build.

Chapter 7. Conclusions and Future Work

Section 7.1 Conclusions

This thesis aimed to accomplish three main goals as stated in the opening section. Those three goals identified goals were to:

- Develop a standard process for identifying machine set points and build parameters for materials new to the Selective Laser Sintering Process
- Determine processing parameters for the Selective Laser Sintering of Carbon Fiber Reinforced Polyetheretherketone
- Improve correlation techniques for predicting mechanical strength of a part based on its thermal history during fabrication

The first goal was accomplished through the development of parameters for Carbon Fiber Reinforced PEEK. After verifying that the powder size was suitable for SLS, techniques were discussed for determining the material's sintering window via Differential Scanning Calorimetry. Visual sintering tests were then utilized to find preheat temperature values and two laser powers to be further investigated. A build matrix was established with those parameters and subsequent builds were run. Post build analysis was then performed to assess the quality of the builds and pick the best laser parameters for building in the CFR PEEK material. This process can be applied for developing build parameters for any new material to the SLS process.

Through the application of the first objective discussed above, the second goal to determine the best build parameters for CFR PEEK was accomplished. The process for determining build parameters was followed and four test builds were conducted. The resulting tensile strengths from the builds were analyzed and a best set of building parameters and set points were determined. These parameters and set points are summarized in Table 3 below.

Table 3. Best build parameters for SLS of CFR PEEK

Laser Power	Scan Speed	Jump Speed	Scan Delay	Jump Delay	Hatch Spacing	Laser On/Off Delay
16.2 W	1500 mm/s	1500 mm/s	1500 mm/s	700 mm/s	300 um	900 us

The third and final objective was to improve correlation techniques between collected MWIR thermal data and the measured tensile strength of the built parts. Previously used correlations techniques (post-sintering temperature) were very poor and do not allow for accurate predictions of tensile strength based on input temperature data. In order to accomplish this, two new methods were used to correlate thermal data with measured mechanical strengths from the CFR PEEK tensile bar builds (Absolute minimum post-sintering temperature and the minimum average post-sintering temperature). R^2 values were used as a quantitative means of comparison for the different methods. On the next page, Table 4 summarizes the three methods and their results when analyzing build 4. Build 4 is chosen as the final means of comparison as it was the build with the best parameters for building in CFR PEEK.

Table 4. Comparison of R^2 values for different analysis methods

Analysis Method	R-Squared Value
Average Post-Sintering Temperature	0.2921
Absolute Minimum Sintering Temperature	0.4088
Minimum Average Sintering Temperature	0.5344

For modeling and predicting output tensile strength, the minimum average post-sintering temperature gave the highest R^2 value for build 4 of .5344. Additionally, this is supported by this same method giving the highest correlation values for builds 2 and 3 as well. It can be seen that this minimum average post-sintering temperature gives a significantly higher correlation than other methods and begins to describe a large amount of the variation in the data. With this quantitative support, it is concluded that the minimum average post-sintering temperature improves upon previous correlation techniques and should be utilized in future analysis when trying to predict the tensile strength of a part built via SLS.

Section 7.2 Future Work

Several tasks can be identified to move forward with stemming from the tasks and conclusions of this thesis. The standardized process for developing parameters in Selective Laser Sintering should be tested with other novel materials. Through multiple trials the process can be further refined and adapted to meet any additional needs of even more unique materials than CFR PEEK. Furthermore, a second build matrix should be constructed for CFR PEEK utilizing even higher laser powers than used in this thesis. The limitations of the laser and optical system prevented the use of higher laser powers. On the other hand, the laser fluence, or total energy input to the parts, could be increased by means other than increasing laser power. A decrease in scan speed could increase the total laser fluence put into the part, leading to the deposition of more energy and potentially better parts.

The final task for future work is the further exploration of correlation measures for thermal data to output mechanical strengths. Utilizing the minimum average post-sintering temperatures will enhance prediction capabilities but there is still further progress to be made. Understanding and modeling the remaining variation and attaining much higher R^2 values is vital to accurately predicting tensile strengths based off of collected thermal data. This improvement will ultimately lead to the ability to create production quality parts with consistently predictable tensile strengths necessary for detailed mechanical design.

Bibliography

Beaman Jr., J. J., & Deckard, C. (1990). *Patent No. 4,938,816.*

Booth, R. B. (2013). *HP3-CF(10) MSDS.* MSDS, Advanced Laser Materials.

Chen, P., Tang, M., Zhu, L., Wen, S., Yan, C., Ji, Z., et al. (2018). Systematical mechanism of Polyamide-12 aging and its microstructural evolution during laser sintering. *Polymer Testing* , 370-379.

Drechsler, K., Heine, M., Medina, L., & Mitschang, P. (2016). *Carbon Fiber Reinforced Polymers.*

Edmund Optics Inc. (2018). *EO-1312M ½" CMOS Monochrome USB Camera.* Retrieved August 6, 2018, from Edmund Optics: https://www.edmundoptics.com/cameras/usb-cameras/eo-usb-2-0-cmosmachine- vision-cameras/59365/

FLIR. (2018). *FLIR A6700sc MWIR Datasheet.* Retrieved August 8, 2018, from FLIR Research & Science: http://www.flir.com/science/display/?id=67022

FLIR Systems, I. (2013). SC8240 User's Manual. Nashua, NH: FLIR Systems, Inc.

Joven, R. (2012). Thermal properties of carbon fiber/epoxy composites with different   fabric weaves.

nanoScience Instruments. (2018). *Scanning Electron Microscopy.* Retrieved August 4, 2018, from nanoScience Instruments: https://www.nanoscience.com/techniques/scanning-electron-microscopy/

Palermo, E. (2013, August 13). *What is Selective Laser Sintering?* Retrieved August 16, 2018, from LiveScience: https://www.livescience.com/38862-selective-laser-   sintering.html

Polymer Science Learning Center. (2018). *Differential Scanning Calorimetry.* Retrieved: August 2, 2018, from Polymer Science Learning Center: http://pslc.ws/macrog/dsc.htm

Rock West Composites. (2018). *Carbon Reinforced PEEK.* Retrieved August 10, 2018, from R ock West Composites: https://www.rockwestcomposites.com/plates-panels-angles/carbon-fiber-plate/cf-peek

Schmid, M., Amado, A., & Wegener, K. (2016). Polymer powders for selective laser sintering (SLS). *AIP Conference Proceedings.* American Institute of Physics.

Skirbutis, G., Dzingute, A., Masiliunaite, V., Sulcaite, G., & Zilinskas, J. (2017). A review of PEEK polymer's properties and its use in prosthodontics. *Baltic Dental and Maxillofacial Journal* , 19-23.

Spears, T. G., & Gold, S. A. (2016). In-process sensing in selective laser melting (SLM) additive manufacturing. *Integrating Materials and Manufacturing Innovation* .

Stone, B., Scibilia, B., Pammer, C., Steele, C., & Keller, D. (2013). *Regression Analysis: How Do I Interpret R-squared and Assess the Goodness-of-Fit?* Retrieved August 2, 2018, from   The Minitab Blog: http://blog.minitab.com/blog/adventures-in-statistics-2/regression-analysis-how-do-i-interpret-r-squared-and-assess-the-goodness-of-fit

Wroe, W. W., Gladstone, J., Phillips, T., Fish, S., Beaman, J., & McElroy, A. (2016). In-situ thermal image correlation with mechanical properties of nylon-12 in SLS. *Rapid Prototyping Journal* , 794-800.